Hartmann wave-front measurement at 13.4 nm with $\lambda_{EUV}/120$ accuracy

Pascal Mercère

Laboratoire d'Interaction du Rayonnement X avec la Matière, Bâtiment 350, Université Paris-Sud, 91405 Orsay, France, and Imagine Optic, 18 Rue Charles de Gaulle, 91400 Orsay, France

Philippe Zeitoun, Mourad Idir, and Sébastien Le Pape

Laboratoire d'Interaction du Rayonnement X avec la Matière, Bâtiment 350, Université Paris-Sud, 91405 Orsay, France

Denis Douillet

Laboratoire d'Optique Appliquée, École Nationale Supérieure des Techniques Avancées, École Polytechnique, Chemin de la Hunière, 91761 Palaiseau, France

Xavier Levecq, Guillaume Dovillaire, and Samuel Bucourt

Imagine Optic, 18 Rue Charles de Gaulle, 91400 Orsay, France

Kenneth A. Goldberg, Patrick P. Naulleau, and Senajith Rekawa

Center for X-Ray Optics, Ernest Orlando Lawrence Berkeley National Laboratory, 1 Cyclotron Road, Berkeley, California 94720

Received February 12, 2003

We report, for the first time to our knowledge, experimental demonstration of wave-front analysis via the Hartmann technique in the extreme ultraviolet range. The reference wave front needed to calibrate the sensor was generated by spatially filtering a focused undulator beam with 1.7- and 0.6-μm-diameter pinholes. To fully characterize the sensor, accuracy and sensitivity measurements were performed. The incident beam's wavelength was varied from 7 to 25 nm. Measurements of accuracy better than $\lambda_{EUV}/120$ (0.11 nm) were obtained at $\lambda_{EUV} = 13.4$ nm. The aberrations introduced by an additional thin mirror, as well as wave front of the spatially unfiltered incident beam, were also measured.

OCIS codes: 120.3940, 120.5050, 120.6650, 260.7200, 220.3740.

To enable metrology and alignment of extreme ultraviolet (EUV) optical systems and to develop next-generation EUV lithography steppers, it is essential that wave-front measurement in this range of wavelengths can be performed rapidly, reproducibly, and accurately. To date, the highest-accuracy wave-front measurements at EUV wavelengths have been obtained with interferometry. On the Advanced Light Source (ALS) beamline 12.0 at Lawrence Berkeley National Laboratory such experiments are routinely performed with accuracy in the $\lambda_{EUV}/250$ range and sensitivity exceeding $\lambda_{EUV}/1000$ ($\lambda_{EUV} = 13.4$ nm) within a 0.1 numerical aperture (NA).[1–4]

However, the Hartmann technique presents some important advantages over interferometry. With the Hartmann wave-front sensor (HWS) both intensity and phase are measured at the same time. HWS can work with spatially and temporally partially incoherent beams. Any kind of optics, focusing or otherwise, with large or small aberrations, can be measured. Finally, HWS is compact, inexpensive, and easy to set up.

In Hartmann wave-front analysis a beam passes through a hole array and is projected onto a CCD camera that detects the beamlet sampled by each hole. The positions of the individual spot centroids are measured and compared with reference positions. This enables the wave front's local slope to be measured at a large number of points within the beam, from which the wave front can be reconstructed.[5] To establish accuracy, a HWS needs to be calibrated with the help of a well-known reference wave. Typically this wave is obtained by spatial filtering.

ALS beamline 12.0 is an undulator beamline designed for experiments relevant to the development of EUV lithography near the 13-nm wavelength.[6] The geometry of ALS beamline 12.0 and the HWS setup are represented schematically in Fig. 1. The undulator beam passes through a varied-line-spacing grating monochromator. The monochromatic EUV beam is focused by Kirckpatrick–Baez (KB) optics with an output-side NA of approximately 0.006. The dimensions of the focal spot are typically 10 μm × 15 μm FWHM.[3,7] The reference spherical wave front needed for the HWS calibration is generated by placing a small pinhole at the focus of the KB optics, creating nominally spherical wave illumination for the HWS.

We used a hole array made in an 80-μm-thick nickel plate composed of a uniform square grid of 65 × 65 holes over a 15 mm × 15 mm area. The holes were square and rotated by 25° to minimize the overlap of the diffraction from adjacent holes in the measurement plane.[8] (Fig. 1).

We used a back-illuminated, thinned, 16-bit EUV CCD camera with 1024 × 1024 pixels. The pixel size was 24 μm × 24 μm. An enlarged part of a typical Hartmann pattern, recorded on the CCD camera with the hole array described above, is also shown in Fig. 1. The diffraction of the beam along the axes of the

0146-9592/03/171534-03$15.00/0

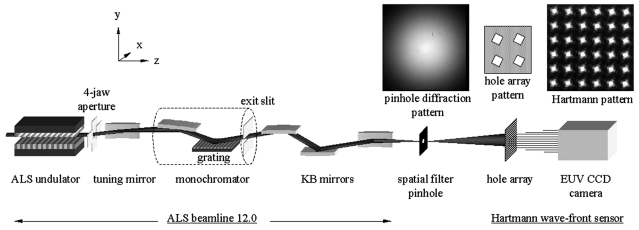

Fig. 1. ALS beamline 12.0 with the spatial filtering and the Hartmann wave-front sensor. Insets, images of the beam diffracted by the pinhole, the hole array pattern, and the Hartmann pattern.

square holes is apparent. The individual spots are approximately 6 pixels (144 μm) wide.

To guarantee a reference wave front better than $\lambda_{\mathrm{EUV}}/100$ rms, the useful pupil of the sensor must be illuminated by less than half of the central Airy disk.[3] For the measurements described here the HWS hole array was placed a distance of 610 mm from the KB focus (NA = 0.025). For this case the pinhole diameter should be 0.6 μm or smaller. However, because of flux limitations imposed by working with such small pinholes,[3] two series of experiments were performed with 1.7- and 0.6-μm pinholes. In both configurations the distances were the same, the operational wavelength was 13.4 nm, and the exposure times were ~150 ms, typically.

Figures 2(a) and 2(b) show the beam's normalized intensity profiles obtained at 13.4 nm with the 1.7- and 0.6-μm pinhole sizes, respectively. With the pinhole of 1.7 (0.6) μm the central Airy disk's diameter is ~11.7 (33.2) mm at the hole array position. In both cases calibration of the sensor was performed over the largest square pupil illuminated (44 × 44 subpupils, where a subpupil defines one individual spot in the Hartmann pattern) centered on the CCD chip. For wave-front analysis we used the largest round pupil inscribed in the beam FWHM, corresponding to a circular analysis pupil of 26 (38) subpupils in diameter (NA ~ 0.0096 and 0.014, respectively).

After calibration of the system we first performed absolute wave-front measurements. Figures 2(c) and 2(d) show the wave-front focus terms obtained with the 1.7- and 0.6-μm pinholes, respectively. In both configurations the diffracted beams are spherical waves with identical radii of curvature, measured by the HWS as 610.161 ± 0.009 mm. Figures 2(e) and 2(f) display the residual wave fronts obtained after removing the tilt and focus terms for the 1.7- and 0.6-μm pinholes, respectively. Finally, the corresponding relative wave fronts are shown in Figs. 2(g) and 2(h). With the pinhole of 1.7 (0.6) μm the residual absolute wave-front rms and peak-to-valley (PV) values reached at best $0.012\lambda_{\mathrm{EUV}}$ ($0.021\lambda_{\mathrm{EUV}}$) and $0.055\lambda_{\mathrm{EUV}}$ ($0.113\lambda_{\mathrm{EUV}}$), respectively. In relative measurement the residual wave front was $0.008\lambda_{\mathrm{EUV}}$ ($0.008\lambda_{\mathrm{EUV}}$) rms and $0.048\lambda_{\mathrm{EUV}}$ ($0.061\lambda_{\mathrm{EUV}}$) PV.

In absolute measurement the magnitudes of the aberrations were larger with the 0.6-μm pinhole than with the 1.7-μm pinhole, because of the larger analysis pupil used with the smaller pinhole size. However, the accuracy measurements were similar with both pinhole sizes, reaching $\lambda_{\mathrm{EUV}}/125$ rms, and a sensitivity of $\lambda_{\mathrm{EUV}}/200$ PV and $\lambda_{\mathrm{EUV}}/1500$ rms were obtained over 50 successive measurements.

We also performed sensitivity measurements by displacing the spatial-filter pinholes in the incident beam, inducing variation of the tilt aberration. Relative to the pinholes' initial positions, the residual wave front did not change significantly ($<\lambda_{\mathrm{EUV}}/500$ rms) for pinhole motions of a few micrometers, and we noted good agreement (within 0.04 μm) between the displacements measured by the sensor (with 0.054-μm precision) and the real ones given by the motorized translation stages (with 0.1-μm precision).

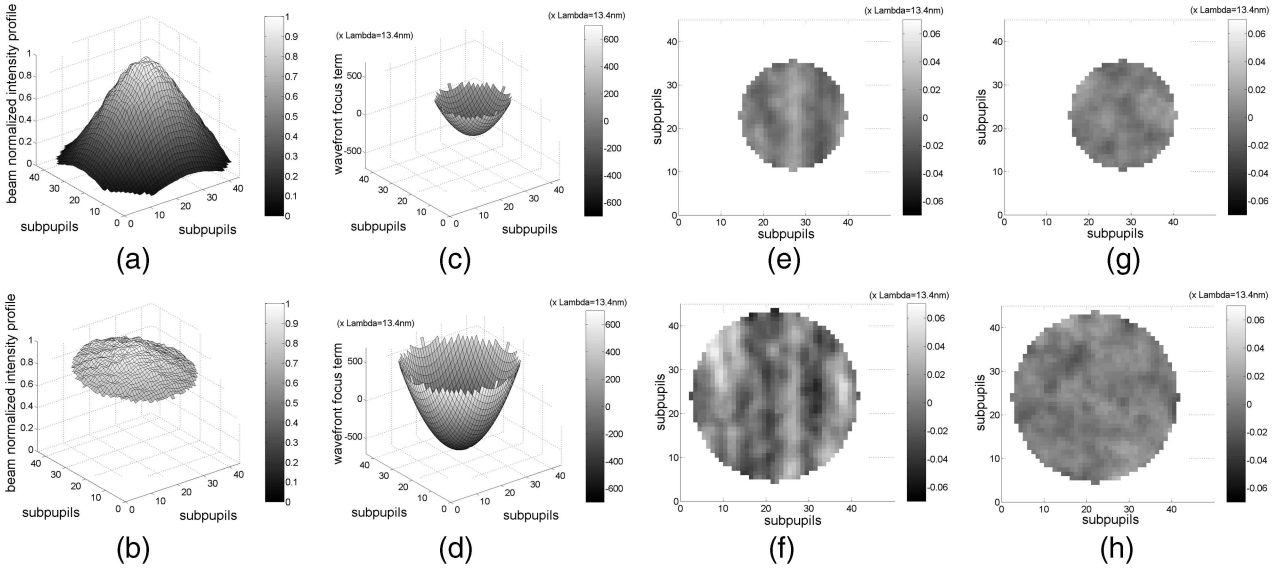

Fig. 2. Normalized beam intensity profiles obtained with (a) the 1.7-μm pinhole and (b) the 0.6-μm pinhole. With the 1.7- and 0.6-μm pinholes, respectively, (c), (d), wave-front focus terms, (e), (f), residual absolute wave fronts, and (g), (h), residual relative wave fronts.

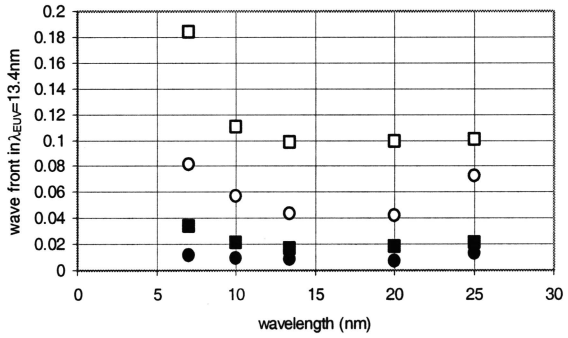

Fig. 3. Wavelength dependence of the residual absolute and relative wave-front measurements in terms of $\lambda_{EUV} = 13.4$ nm over the same analysis pupil with the 1.7-μm pinhole. The full (empty) squares and circles are the absolute and relative rms (PV) wave-front measurements, respectively.

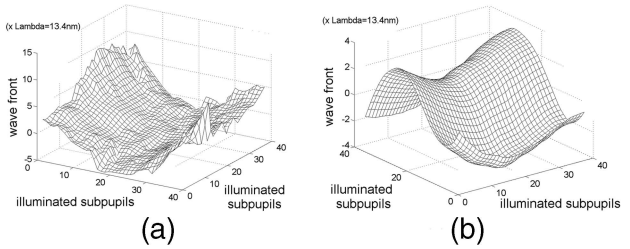

Fig. 4. (a) Wave front reflected by a flat Mo/Si multilayer-coated mirror placed in front of the spatially filtered incident beam. (b) ALS beamline 12.0 wave-front measurement without spatial filtering at 13.4 nm.

On ALS beamline 12.0 the wavelength can be tuned from 7 to 25 nm with a $\lambda/\Delta\lambda$ bandwidth between 55 and 500. Thus we performed, at different wavelengths, absolute and relative wave-front measurements with both pinhole sizes. Here the reference wave front, taken in relative measurements, is always the wave front measured at $\lambda_{EUV} = 13.4$ nm. For many wavelengths the transmission of the 250-nm-thick nickel membrane that defines the 0.6-μm pinhole was too high to provide adequate spatial filtering. Therefore only the results obtained with the 1.7-μm pinhole are considered.

Figure 3 shows the residual rms and PV values obtained at different wavelengths with the 1.7-μm pinhole in terms of $\lambda_{EUV} = 13.4$ nm; comparisons are made between the operational wavelength and the results measured at 13.4 nm, always using the same analysis pupil (i.e., the same measurement NA), corresponding to the FWHM diameter at 13.4 nm. We see that the wave-front measurements performed between 10 and 25 nm are similar; however, the wave-front quality deteriorates rapidly as expected below $\lambda = 10$ nm because the measurement pupil falls outside the FWHM of the central Airy disk. This set of measurements demonstrates the achromaticity of the technique, showing that the HWS can easily work over a wide wavelength range (7–25 nm) without recalibrating the sensor.

As an application of the Hartmann technique, we first measured the wave front reflected by a Mo/Si multilayer-coated mirror. The mirror was positioned, with 67.5° incidence, to reflect the pinhole diffracted beam before it entered the HWS. Figure 4(a) shows the measured wave front reflected by the wafer at $\lambda = 13.4$ nm. The residual rms and PV aberration magnitudes were $2.715\lambda_{EUV}$ and $18.387\lambda_{EUV}$, respectively.

The spatial-filter pinhole was then removed to measure the wave front of the incident beam produced by the KB optics. The wave front, displayed in Fig. 4(b), has residual-aberration magnitudes of $1.879\lambda_{EUV}$ rms and $6.99\lambda_{EUV}$ PV. The primary wave-front error terms are astigmatism, coma at 90°, and trifoil at 30°. By convolution of the calculated point-spread function with the geometrical image of the beamline source, we estimated the size of the KB focal spot at 23 μm × 26 μm at $1/e^2$, while direct imaging gave 21 μm × 25 μm at $1/e^2$. Thus HWS can also predict the focal spot properties of highly aberrated beams.

To our knowledge these experiments are the first to demonstrate the performance of Hartmann wave-front sensing in the EUV wavelength range. We performed EUV Hartmann wave-front sensor calibration and wave-front analysis at 13.4 nm; accuracy better than $\lambda_{EUV}/120$ rms and sensitivity of $\lambda_{EUV}/1500$ rms were obtained. This sensor was also tested on a wide wavelength range, from 7 to 25 nm, without any modification. We characterized the surface deformations of a thin flat mirror, as well as the ALS beamline 12.0 beam focused by KB optics. The EUV HWS can also be used for adaptive or active optics alignment and beam movement sensing on complex optical setups.

The authors are greatly indebted to E. Morcet for enabling the use of the Center for X-Ray Optics's EUV CCD camera with the Imagine Optic Hartmann data treatment software and to members of the Center for X-Ray Optics, including P. Denham, B. Hoef, A. Liddle, B. Harteneck, K. Rosfjord, D. Attwood, and E. Anderson, for their support. P. Mercere's e-mail address is mercere@enstay.ensta.fr.

References

1. P. P. Naulleau, K. A. Goldberg, S. H. Lee, C. Chang, D. Attwood, and J. Boker, Appl. Opt. **38,** 7252 (1999).
2. K. Medecki, E. Tejnil, K. A. Goldberg, and J. Bokor, Opt. Lett. **21,** 1526 (1996).
3. K. A. Goldberg, Ph.D. dissertation (University of California, Berkeley, 1997).
4. E. Tejnil, K. A. Goldberg, S. H. Lee, H. Medecki, P. J. Batson, P. E. Denham, A. A. MacDowell, and J. Bokor, J. Vac. Sci. Technol. B **15,** 2455 (1997).
5. W. H. Southwell, J. Opt. Soc. Am. **70,** 998 (1980).
6. D. Attwood, P. P. Naulleau, K. A. Goldberg, E. Tejnil, C. Chang, R. Beguiristain, P. Batson, J. Bokor, E. M. Gullikson, M. Koike, H. Medecki, and J. H. Underwood, IEEE Quantum Electron. **35,** 709 (1999).
7. D. Attwood, *Soft X-Rays and Extreme Ultraviolet Radiation—Principles and Applications* (Cambridge U. Press, Cambridge, England, 1999).
8. Imagine Optics, patent PCT/FR02/02495 (July 2002).